


Single to multiple acoustic vortex excitations in the transition to defect-mediated dust acoustic wave turbulence

Jun-Yi Tsai,^{1,2} Po-Cheng Lin,¹ and Lin I ¹

¹*Department of Physics and Center for Complex Systems, National Central University, Zhongli, Taiwan 32001, Republic of China*

²*Molecular Science and Technology, Taiwan International Graduate Program, Academia Sinica and National Central University, Taipei, Taiwan 10617, Republic of China*



(Received 15 November 2019; accepted 31 January 2020; published 25 February 2020)

We experimentally investigate the cooperative excitations in the transition from a self-excited three-dimensional ordered plane wave to a defect-mediated turbulence (DMT) state with multiple unstable defect filaments in a dusty plasma system. It is found that, with increasing effective driving, a single acoustic vortex (AV) with positive or negative helicity winding around a long straight defect filament with small wiggling in the $2 + 1D$ (dimensional) space-time space starts to emerge along the center axis of the small dust cluster. The sequential ruptures of the crest surfaces from the cluster boundary followed by their reconnection with adjacent ruptured crest surfaces, or repelling one of the pairwise generated defects out of the boundary, are the key for the single AV generation. Further increasing driving makes the single defect filament exhibit helical excursion in the $2 + 1D$ space. The system eventually enters the state with a few short-lived AVs and the DMT state with multiple AVs. The gradual increasing defect filament fluctuations and defect number in the transition to the DMT more strongly distort the nearby waveforms, which leads to the transition from the emergence of distinct sideband peaks to the broadened peaks in the power spectra of temporal dust density fluctuation. For the system with a larger cluster size, the single AV states are skipped in the transition to the DMT state.

DOI: [10.1103/PhysRevE.101.023210](https://doi.org/10.1103/PhysRevE.101.023210)

I. INTRODUCTION

Under increasing driving, the ordered wave state can be changed to the wave turbulent state through the weakly disordered wave state. It occurs ubiquitously in many extended nonlinear dissipative media, such as acoustic, fluid, plasma, and optical systems [1–6]. For the weakly disordered state, modulation instability can cause waveform undulation with phase and amplitude modulations, and the broadening of the sharp peaks (fundamental and harmonic modes) in the power spectrum for systems governed by nonlinear wave equations such as Landau-Ginzburg or nonlinear Schrödinger equations [7–12]. Fluctuating defects emerge at the troughs of modulation envelopes, where amplitudes are null and phases are undefined. It leads to what is termed defect-mediated turbulence (DMT) for the weakly disordered wave state dominated by a single wavelength scale. For two-dimensional (2D) and three-dimensional (3D) systems, defects appear in the form of fluctuating filaments with various lengths in the $2 + 1D$ and $3 + 1D$ space-time space, respectively [13–16]. Nevertheless, the detailed transition from the ordered plane wave state to the DMT state with many fluctuating defect filaments, especially for the 3D traveling wave and associated spatiotemporal waveform dynamics, remains elusive.

The screw-type dislocation with a helical waveform winding around the defect filament is the fundamental singular excitation in 3D traveling plane waves [17–22]. In acoustic and optical waves, screw dislocations are also called acoustic vortices (AVs) and optical vortices (OVs), respectively [14,17,23]. Their defect filament cores with null amplitudes are also referred to as amplitude hole filaments, the lines

of silence and darkness, respectively [23,24]. In past experimental studies, AVs and OVs have been mainly passively generated, through the interference of waves with the same frequency but different phases excited through passing phase plates or by oscillating driver arrays with programmed phase delay [14,17,19–21].

On the other hand, for the 3D traveling acoustic type wave in the DMT state, recent studies on the self-excited dust acoustic wave (DAW) demonstrated the spontaneous pairwise generation and annihilation of AVs with opposite helicities winding around a pair of defect filaments in $2 + 1D$ space-time space, which conserves the topological charges (AV helicities) and angular momentum [24,25]. The multiscale temporal fluctuations of defect number in xy space following power-law decay in the power spectrum, and the defect filament trajectories with uncertain lengths and motion, manifest in the absence of long-time predictability of defect motion in xyt space [25]. Note that the 2D xy space is the plane normal to the wave propagation direction. The waveform undulation through modulation instability induces sequential rupture and reconnection of adjacent wave crest surfaces. It is the key for the *spontaneous* pairwise generation and annihilation of AVs with opposite helicities, located at the two ends of the rupture and reconnection lines with finite lengths on wave crest surfaces. Those spontaneously excited moving and interacting AVs are the basic coherent excitations for characterizing 3D acoustic-type waveform dynamics [24]. The emergence of those fluctuating defects is also associated with the broadening of the sharp peaks in the power spectrum of the temporal local density fluctuations in the ordered plane wave state [25].

Nevertheless, the previous works were conducted in the DMT state mainly with pairwise defect generation and annihilation [24,25]. The following fundamental issues in the transition from the ordered plane wave state to the DMT state with fluctuating multi-AVs remain unexplored. (A) Is it possible to spontaneously enter a single AV state, which seems to violate topological charge conservation? (B) If yes, what is the generation mechanism? (C) What is the transition scenario from the ordered plane wave state to the above DMT state with multi-AVs? (D) How are the dynamics of mono-AV to multi-AVs and the broadening of the dust density fluctuation spectra correlated?

In this work, the above unexplored fundamental issues are addressed experimentally in self-excited DAWs. Defect filament trajectories and surrounding waveforms in xyt space are tracked, where the xy plane is the plane normal to the wave propagation direction. For the small dust cluster that is 13 mm in diameter, we demonstrate the transition from the ordered plane wave state I to the DMT state V through the emergence of a single AV with helical waveform winding around straight and helical defect filaments (states II and III, respectively; see also Sec. III. C), and a few short-lived AVs (state IV). The gradual loss of the defect filament stability more strongly distorts the surrounding waveforms. It leads to the transition from the emergence of distinct sideband peaks to the broadened peaks in the temporal power spectra of dust density fluctuations. The sequential rupture of wave crest surfaces from the boundary followed by their reconnection with the adjacent ruptured crest surfaces, or repelling one of the pairwise generated AVs to the boundary, is the key for the single AV generation. If the dust cluster diameter is increased to more than 15 mm, the system skips the single AV states II and III before the transition to states IV and V from the ordered plane wave state.

The DAW, also called the dust density wave, associated with the longitudinal oscillations of negatively charged micrometer-sized dust particles in the low-pressure plasma, is an acoustic-type density wave [26–34]. It can be self-excited in the laboratory plasma system through the interplay of dust inertia, screened Coulomb interaction, and ion streaming [29,30]. This fundamental acoustic-type density wave, with dynamics governed by modulation-type nonlinear dynamical equations [35], has been widely used to investigate many ubiquitous dynamical behaviors of nonlinear waves. Shock waves [36], solitary waves [37], wave-breaking [27], wave-particle interaction [27], defects [24,25,32], AVs [24], rogue waves [38], and wave turbulence [34,39] are good examples. Especially, the proper dust particle size and spatiotemporal dynamical scales allow us to explore spatiotemporal waveform dynamics in $2 + 1D$ space-time space through visualizing large-area dusty density evolution illuminated by a laser sheet [24].

II. EXPERIMENT SETUP

The experiment is conducted in a cylindrical symmetric rf dusty plasma system, similar to our previous experiment [27], as sketched in Fig. 1(a). The weakly ionized glow discharge ($n_e \sim 10^9 \text{ cm}^{-3}$) is generated in an argon/oxygen gas mixture using a 14-MHz rf power system operated at

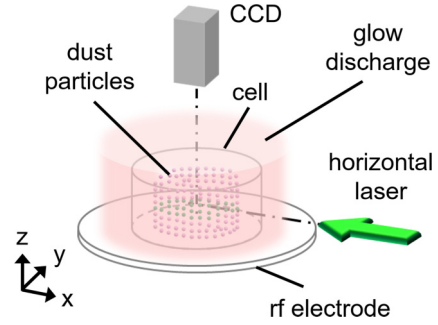


FIG. 1. Sketch of the experimental setup, similar to our previous experimental setup [27].

2.3 W. A hollow cylindrical glass with 25 mm inner diameter is put on the center of the bottom electrode to confine dusty plasma with MF (melamine-formaldehyde) particles ($5.3 \mu\text{m}$ in diameter, $1.1 \times 10^{-10} \text{ g}$ in mass, and 1.5 g/cm^3 density). The estimated Debye length λ_D and dust particle charges are in the order of a few tens of micrometers and a few to ten thousands of electrons per particle, respectively. The system is fine-tuned from the ordered plane wave state to the DMT state by decreasing oxygen partial pressure. Note that in the argon/oxygen mixture, the formation of negative oxygen ions can reduce the loss rate of negatively charged species because of the much lower mobility of negative oxygen ions than that of electrons [40]. It thereby reduces the plasma floating potential with respect to the electrode and consequently reduces the ion streaming to drive DAWs. Namely, the system can be tuned to the more disordered state by decreasing oxygen pressure.

The top view image of dust particles illuminated by an extended laser sheet in the horizontal (xy) plane is captured by a charged-coupled device at 400 Hz sampling rate. The normalized local dust density $n_d(x, y, t)$ is obtained by measuring the coarse-grained image brightness with a Gaussian weighted circle (0.3 mm full width at half-maximum), normalized by its temporal average. For identifying defect filaments and plotting the wave crest surfaces of the surrounding defects, the amplitude and phase are obtained through Hilbert transform of the fundamental mode from band-pass filtered (from 22 to 50 Hz) local dust density $n_d(x, y, t)$, similar to our previous study [24,25].

III. RESULTS AND DISCUSSION

A. Transition from the plane wave state to the DMT state

Let us first start from the results using a dust cluster 13 mm in diameter. Figures 2(a) and 2(b) show the spatiotemporal waveforms of n_d and their corresponding defect trajectories in the xyt space of states I to V, at oxygen partial pressure $P_O = 60, 55, 49, 43,$ and 34 mTorr , respectively, and constant argon pressure at 240 mTorr . With decreasing oxygen pressure, the increasing modulation instability causes waveform undulation. The transition from the defect-free plane wave state I to the multidefects (multi-AVs) state V with increasing degrees of disorder runs through the following three intermediate states: (a) state II with a single straight defect filament exhibiting small amplitude wiggling at the

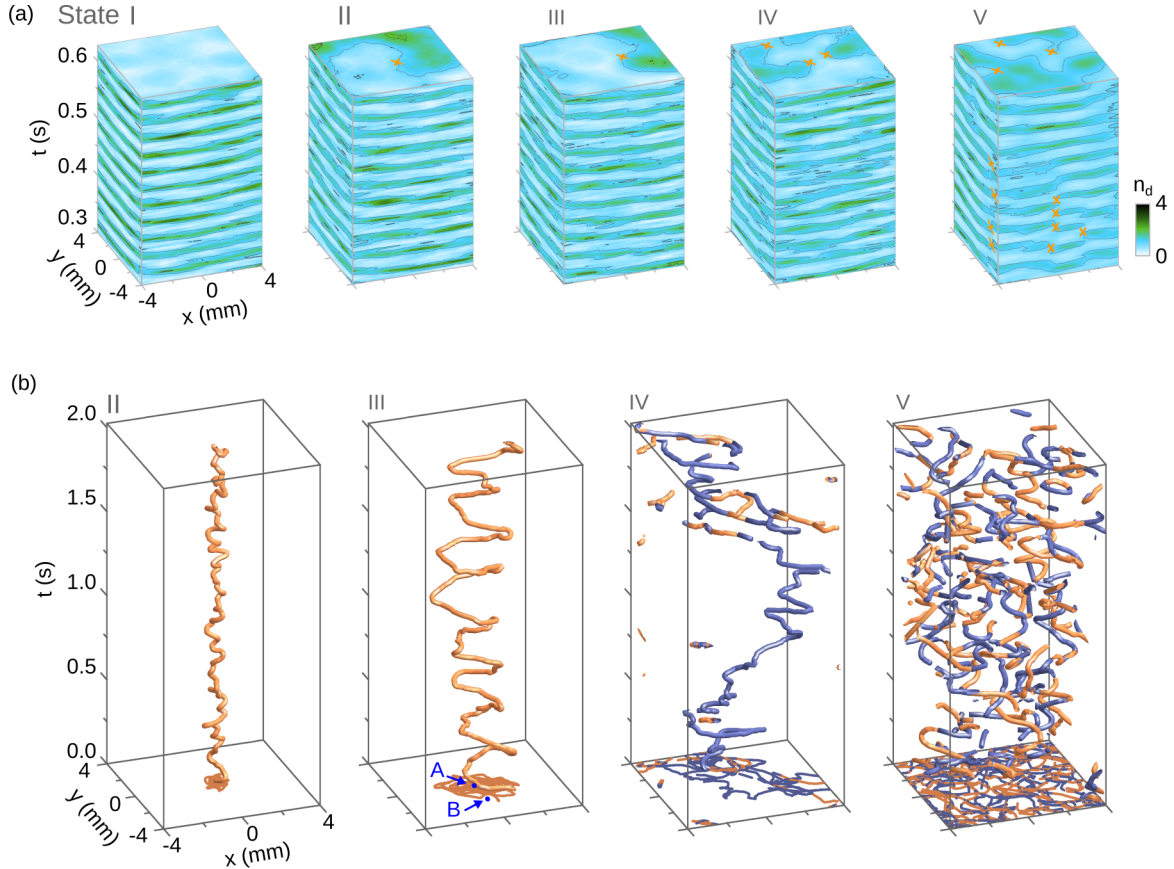


FIG. 2. (a) and (b) Color-coded plots of n_d on the xy , xt , and yt planes and defect filaments in the xyt space, showing the transition from the defect-free plane wave state I to the weakly disordered wave state V (DMT state), through state II with a single defect filament exhibiting small amplitude wiggling, state III with a single helical defect filament, and state IV with a single to few chaotic defect filaments. The crosses in (a) label defect locations with null amplitudes and undefined phases. The orange and blue defect filaments (trajectories) in (b) represent the left- and right-handed helicities of the surrounding AVs, respectively. Their corresponding projections on the bottom xy plane are also plotted. In (a) and (b), the panels in the same row share the same spatial and temporal scales.

dust cluster center, (b) state III with a single defect filament exhibiting large amplitude unstable helical excursion around the cluster center, and (c) state IV with intermittent emergence of a single or few short-lived defect filaments in the xyt space. Obviously, the longtime predictability of the defect filament is poor in states IV and V due to the uncertain lifetime and motion of the defect, similar to those observed in our previous experiment [25]. However, the stable defect filament with a long lifetime of state II manifests in long-time predictability. In state III, although the defect lifetime is also very long, the defect predictability is deteriorated due to the unstable helical motion of the defect filament.

Figure 3 shows the typical waveforms of wave crest surfaces surrounding the defects in states II–IV. The single AV with either a left- or right-handed helical waveform winding around the single defect filament can be sustained in states II [see Figs. 3(a) and 3(b)] and III. The above single AV generation breaks the right-left-handed symmetry through the spontaneous symmetry breaking process depending on the details of the wave surface fluctuations in the initial forming stage.

Figures 4(a) and 4(b) show the temporal evolution of n_d at points A and B, located at the dust cluster center and 2 mm from the center [see their locations on the bottom plane of

state III in Fig. 2(b)] of different states, and the corresponding waterfall plots of the power spectra averaged over a circular area 8 mm in diameter and centered at point A, respectively. Increasing effective driving causes modulation of the dust density oscillation. It makes the spatially averaged power spectra of local dust density evolution exhibit (a) distinct narrow peaks of fundamental and harmonic modes in state II, (b) the emergence of sideband peaks in state III, and (c) gradual broadening of fundamental and harmonics peaks in states IV and V.

B. Correlation between fluctuating defects and the power spectra of local dust density fluctuations

Now, let us focus on the dynamics of fluctuating defects and their correlation with the averaged power spectra of local dust density fluctuations of each state.

State II is the state with a single straight defect filament exhibiting small amplitude wiggling, located around the center point A of the xy plane [Fig. 2(b)]. Since the wave amplitude is null and small at and around the defect location, respectively, the small amplitude wiggling of the defect trajectory (defect filament) in the xyt space (also see its trajectory in the xy plane) makes $n_d(t)$ at point A exhibit small amplitude

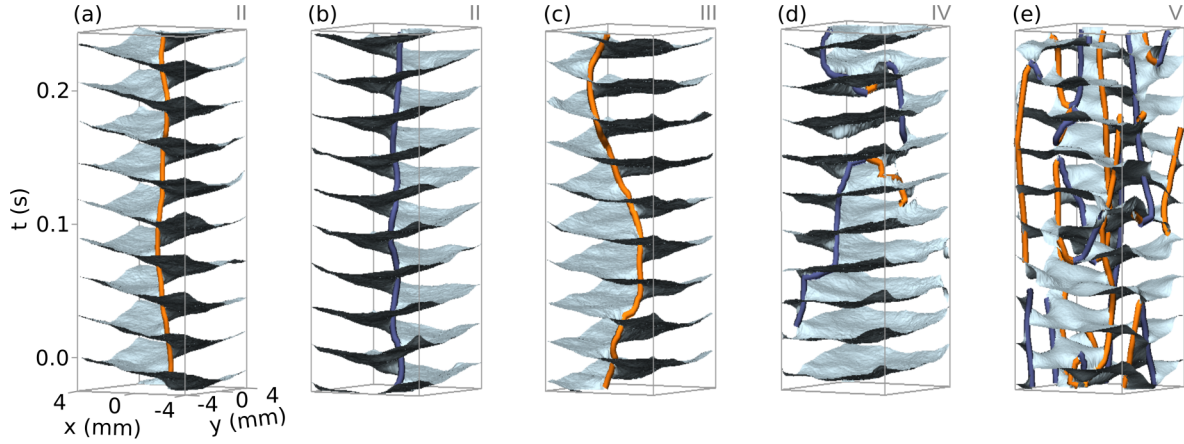


FIG. 3. Stereo waveforms of wave crest surfaces winding around the orange and blue defect filaments in the xyt space, representing the left- and right-handed helicities of states II to V, respectively. Either a left- or right-handed single AV can be spontaneously excited in state II [e.g., (a) and (b), respectively] and state III (not shown). The same spatial and temporal scales are used in plotting for all the waveforms.

temporal fluctuations [Fig. 4(a)]. However, at point B, 2 mm away from point A, $n_d(t)$ exhibits stable oscillations similar to that in state I at point A. It also causes the sharp fundamental and harmonics of the spatially averaged n_d spectrum over the xy space of state II, which are similar to those of state I [Fig. 4(b)]. Figure 5(c) further shows the power spectra of $X(t)$ and $Y(t)$, where (X, Y) is the defect location in the xy plane. The defect trajectory spectra exhibit turbulent-like spectra with weak intensity and a widespread descending tail.

As shown in Fig. 2(b), in state III, the single defect exhibits large helical motion in the xyt space (also see its excursion trajectory in the xy plane). The power spectra of $X(t)$ and $Y(t)$ in Fig. 5(c) both show a broad bump peaked at $f_d = 4.2$ Hz, associated with a high-frequency tail exhibiting a power-law decay. Since the amplitude of n_d gradually decreases with the decreasing distance to the defect filament, the wave crest surface winding around the helical defect filament [see Fig. 3(c)] also causes the amplitude modulation of n_d at both

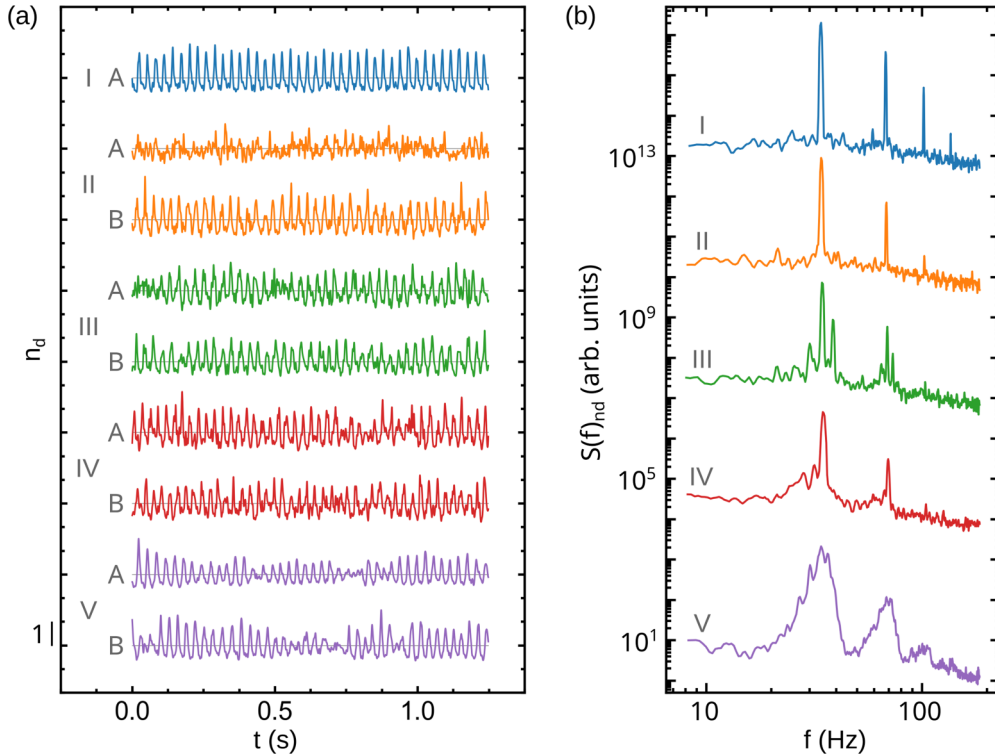


FIG. 4. (a) Temporal evolution of $n_d(t)$ at points A and B, located at the dust cluster center and 2 mm from the center, respectively [see their locations on the bottom xy plane of state III in Fig. 2(b)] from states I to V. (b) Waterfall plots of the corresponding averaged power spectra of the local $n_d(t)$ over a circular area 8 mm in diameter and centered at point A. The defect trajectories determine the surrounding helical waveforms, which modulate dust density and consequently determine how the sharp peaks in the dust density power spectra are broadened.

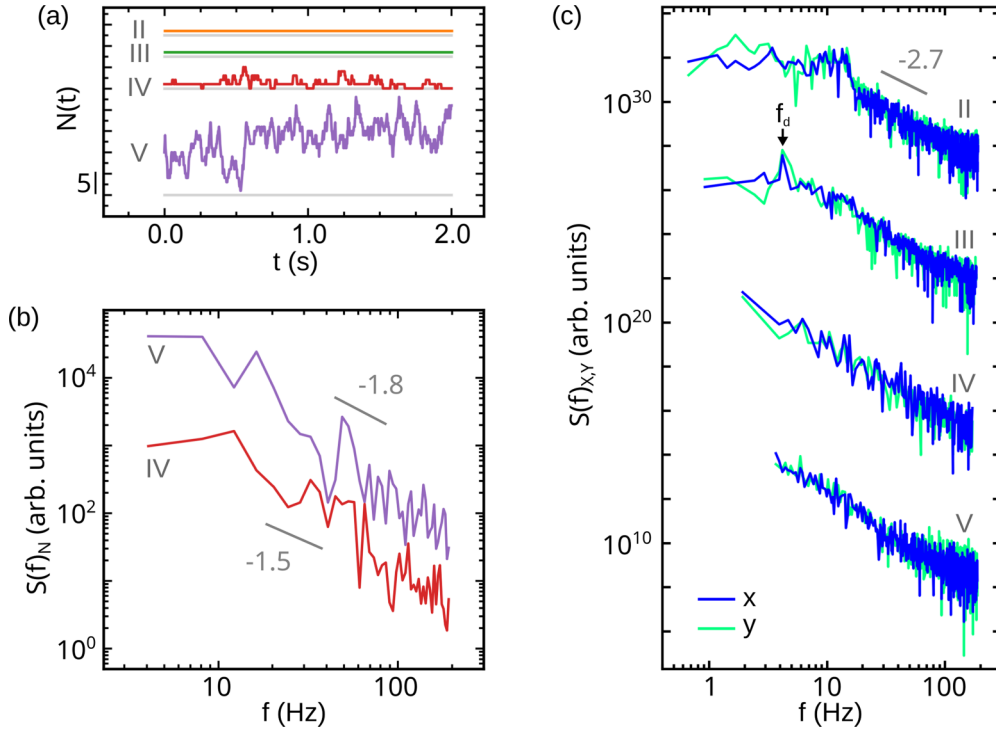


FIG. 5. (a) Temporal evolution of total defect number $N(t)$ in a circular area 8 mm in diameter and centered at the xy plane, for states II to V. The gray lines indicate the zero level of defect number. (b) Power spectra of $N(t)$ for states IV and V. (c) Waterfall plots of the power spectra of $X(t)$ (blue) and $Y(t)$ (cyan) for states II to V, where (X, Y) is the defect location in the xy plane. In state III, the dominant frequency is labeled by f_d . The numbers by the gray lines in (b) and (c) indicate the scaling exponents of the descending tails in the power spectra.

points A and B [Fig. 4(a)]. Unlike the averaged n_d spectrum of state II, two distinct sideband peaks emerge in each sharp peak of the fundamental and harmonics of the averaged n_d spectrum state III, with a 4.2 Hz spectrum band gap, which coincides with the bump peaked at f_d in the defect trajectory spectrum [Fig. 5(c)]. Namely, the helical defect filament with a dominant gyrating frequency f_d in the xy space is associated with the amplitude modulation of $n_d(t)$, which consequently causes the emergence of the distinct sideband peaks adjacent to the main peaks in the n_d spectrum.

In state IV, a single to a few short-lived defects with chaotic trajectories in the xy space can be intermittently excited [see Fig. 5(a) for the temporal evolution of defect number $N(t)$ inside a center circle 5.5 mm in radius], which is associated with the highly fluctuating n_d at both points A and B [Fig. 4(a)]. Comparing with state III, the more chaotic defect trajectories lead to the extension of the scale-free power spectrum of defect trajectories to the lower frequency end [Fig. 5(c)]. It consequently induces more chaotic modulation on the stereo waveform [Fig. 3(d)] and the oscillating n_d at all points [e.g., see Fig. 4(a)], and in turn smears out the sharp sidebands and the main peaks of the fundamental and the second harmonic modes in the averaged n_d spectrum [Fig. 4(b)].

The system enters the DMT state V with a strong fluctuation of defect number around the higher averaged defect number (13 in a circle 5.5 mm in radius of the xy space) [Fig. 5(a)], associated with the stronger modulation on the stereo waveform [Fig. 3(e)] and the oscillating n_d in both points A and B [Fig. 4(a)]. Comparing with state IV, the power spectrum of the temporal defect number fluctuation of state

V also exhibits a steeper spectrum extending to the lower frequency end [Fig. 5(b)]. The more chaotic defect trajectories with shorter lifetimes lead to the absence of the low-frequency part in $S(f)_{X,Y}$. It consequently further enhances the broadening of the fundamental and second harmonic in the n_d power spectrum comparing with those of state IV [Fig. 4(b)].

C. Single AV generation mechanism

As reported in our previous work, modulation instability leads to crest surface undulation [25]. In the DMT state, initiated with the formation of a kink with a finite length on the crest surface, the trailing crest surfaces are ruptured along with the kink sequentially [Fig. 6(a)]. The sequential reconnection of the upward bending crest surface with the downward bending part of the trailing ruptured crest surfaces along the kink line heals the ruptured crest surfaces. It causes the formation of a pair of AVs with opposite helicities winding around the pair of defect filaments at both ends of the ruptured and reconnected crest surfaces. Through the opposite process, a defect can annihilate with its twin brother or another defect with opposite helicity from another pair generation process. In the above pair generation and annihilation processes, the overall topological charges (helicity of AVs) in the system are conserved.

How can a single defect be generated in states II and III? As shown in Fig. 6(b), it can be first generated through the pair generation similar to the above process, followed by the escaping of one defect to the cluster boundary [41]. It can also be generated starting from rupturing the crest surface from the dust cluster boundary, followed by the sequential crest

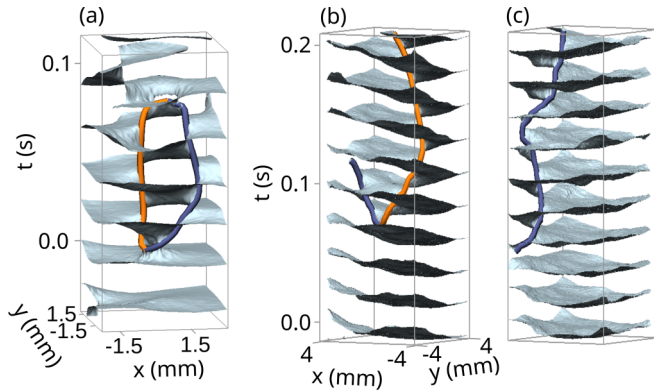


FIG. 6. (a) Stereo waveforms of the wave crest surfaces around pairwise generated and annihilated defects with opposite helicities in state V. See our previous report [24] for more details. (b) and (c) Generation of the single defect filament by repelling one of the pairwise generated AVs to the cluster boundary, and by rupturing crest surfaces from the cluster boundary followed by crest surface reconnection, respectively. The same spatial and temporal scales are used in plotting (b) and (c).

rupture and reconnection of trailing crest surfaces [Fig. 6(c)]. Namely, the spontaneous symmetry breaking process through one of the above two processes is the key for a single defect generation process, which leaves a net topological charge in the system. The spontaneous symmetry breaking of defect charge (AV helicity) is determined by the initial forming condition of wave surface fluctuations.

Note that the above results from Figs. 2–6 are obtained from a dust cluster 13 mm in diameter. However, for clusters with diameters larger than 15 mm, the system directly changes from the ordered plane wave state I to states IV and V by skipping states II and III each with a single long-lived defect. The larger dust clusters can more easily allow long wavelength modes to modulate waveforms. It causes the spontaneous generation of a few defects followed by multidefects, even with the slight increase of effective driving from that of the ordered plane wave modes. Namely, for a larger dust cluster, the boundary plays a less important role for defect absorption and crest rupturing, which are the two keys for entering a single defect state. Similar boundary effects on defect absorption were also reported in different open dissipative systems such as confined active nematics and cardiac scroll waves [41,42].

IV. CONCLUSION

In conclusion, by tuning the effective driving in DAWs, we experimentally demonstrate the transition from the plane

wave state I to the weakly disordered DMT state V with multiple fluctuating defects, through the three intermediate states: (a) state II with a single stable defect filament exhibiting small amplitude wiggling, (b) state III with a single filament exhibiting helical excursion at dominant frequency, and (c) state IV with few defect filaments. Each defect filament is wound around by the acoustic vortex with helical waveform. Repelling one of the pairwise generated AVs (defects) to the cluster boundary or the sequential rupture of the crest surfaces from the cluster boundary followed by crest surface reconnection to the adjacent ruptured crest surfaces is the key for generating a single AV in states II and III. The detailed initial waveform fluctuations in the above spontaneous symmetry breaking process of AV generation determines the sign of AV helicity.

In state II, the ordered waveform of the stable AV winding around the straight defect filament still sustains the ordered dust density fluctuation and the sharp peaks without sideband peaks in the dust density spectra for the region away from the defect filament core. In state III, the helical defect filament with the dominant defect gyrofrequency f_d causes amplitude modulation of dust density. It in turn induces the sideband peaks with frequency gap f_d from the fundamental and harmonic peaks in the averaged n_d spectrum. In state IV, AVs winding around defect filaments with more chaotic excursion and shorter lifetimes smear out the dominate peaks in the scale-free trajectory spectrum. It causes more chaotic modulation of $n_d(x, y, t)$, and consequently leads to the broadening of fundamental and second harmonic modes in the averaged n_d power spectrum.

Increasing the dust cluster diameter to larger than 15 mm allows a long wavelength mode for waveform modulation. It consequently makes the system more vulnerable for multiple defect generation. The system changes from the ordered plane wave state directly to the state IV with few short-lived defects and the DMT state V with multi-short-lived defects by skipping the states II and III each with a long-lived single defect under increasing driving.

Our study sheds light on the transition dynamics from the plane wave state to the DMT state through the intermediate states with a single AV to few AVs, especially the dynamical origin for single AV generation. It paves the way for future experimental and theoretical studies on nonlinear acoustic type waves in various nonlinear media.

ACKNOWLEDGMENTS

This work is supported by the Ministry of Science and Technology, Taiwan, under Contract No. MOST-108-2112-M-008-015.

[1] M. V. Goldman, *Rev. Mod. Phys.* **56**, 709 (1984).
 [2] E. Falcon, C. Laroche, and S. Fauve, *Phys. Rev. Lett.* **98**, 094503 (2007).
 [3] A. N. Ganshin, V. B. Efimov, G. V. Kolmakov, L. P. Mezhov-Deglin, and P. V. E. McClintock, *Phys. Rev. Lett.* **101**, 065303 (2008).
 [4] H. Punzmann, M. G. Shats, and H. Xia, *Phys. Rev. Lett.* **103**, 064502 (2009).

[5] E. G. Turitsyna, S. V. Smirnov, S. Sugavanam, N. Tarasov, X. Shu, S. A. Babin, E. V. Podivilov, D. V. Churkin, G. Falkovich, and S. K. Turitsyn, *Nat. Photon.* **7**, 783 (2013).
 [6] D. Pierangeli, F. DiMei, G. DiDomenico, A. J. Agranat, C. Conti, and E. DelRe, *Phys. Rev. Lett.* **117**, 183902 (2016).
 [7] Q. Ouyang and J. M. Flesselles, *Nature (London)* **379**, 143 (1996).

- [8] I. S. Aranson and L. Kramer, *Rev. Mod. Phys.* **74**, 99 (2002).
- [9] G. Prasad, J. Pramanik, B. M. Veerasha, A. Sen, and P. K. Kaw, in *Dusty Plasmas in the New Millennium: Third Conference on the Physics of Dusty Plasmas*, edited by R. Bharuthram, M. A. Hellberg, P. K. Shukla, and F. Verheest, AIP Conf. Proc. No. 649 (AIP, New York, 2002), pp. 231–234.
- [10] A. S. Mikhailov and K. Showalter, *Phys. Rep.* **425**, 79 (2006).
- [11] O. Kimmoun, H. C. Hsu, B. Kibler, and A. Chabchoub, *Phys. Rev. E* **96**, 022219 (2017).
- [12] A. E. Kraych, P. Suret, G. El, and S. Randoux, *Phys. Rev. Lett.* **122**, 054101 (2019).
- [13] P. Couillet, L. Gil, and J. Lega, *Phys. Rev. Lett.* **62**, 1619 (1989).
- [14] F. T. Arecchi, G. Giacomelli, P. L. Ramazza, and S. Residori, *Phys. Rev. Lett.* **67**, 3749 (1991).
- [15] I. Freund and N. Shvartsman, *Phys. Rev. A* **50**, 5164 (1994).
- [16] M. V. Berry and M. R. Dennis, *Proc. R. Soc. London, Ser. A* **456**, 2059 (2012).
- [17] H. He, M. E. J. Friese, N. R. Heckenberg, and H. Rubinsztein-Dunlop, *Phys. Rev. Lett.* **75**, 826 (1995).
- [18] S. Alonso, F. Sagués, and A. S. Mikhailov, *Science* **299**, 1722 (2003).
- [19] X. Jiang, Y. Li, B. Liang, J. C. Cheng, and L. Zhang, *Phys. Rev. Lett.* **117**, 034301 (2016).
- [20] H. Esfahlani, H. Lissek, and J. R. Mosig, *Phys. Rev. B* **95**, 024312 (2017).
- [21] J. L. Thomas and R. Marchiano, *Phys. Rev. Lett.* **91**, 244302 (2003).
- [22] P. K. Shukla, *Phys. Plasmas* **19**, 083704 (2012).
- [23] K. O’Holleran, M. R. Dennis, and M. J. Padgett, *Phys. Rev. Lett.* **102**, 143902 (2009).
- [24] Y.-Y. Tsai and L. I, *Phys. Rev. E* **90**, 013106 (2014).
- [25] M. C. Chang, Y. Y. Tsai, and L. I, *Phys. Plasmas* **20**, 083703 (2013).
- [26] N. N. Rao, P. K. Shukla, and M. Y. Yu, *Planet. Space Sci.* **38**, 543 (1990).
- [27] L. W. Teng, M.-C. Chang, Y.-P. Tseng, and L. I, *Phys. Rev. Lett.* **103**, 245005 (2009).
- [28] J. H. Chu and Lin I, *J. Phys. D* **27**, 296 (1993).
- [29] M. R. Amin, G. E. Morfill, and P.-K. Shukla, *Phys. Rev. E* **58**, 6517 (1998).
- [30] R. L. Merlino, *Phys. Plasmas* **16**, 124501 (2009).
- [31] K. O. Menzel, O. Arp, and A. Piel, *Phys. Rev. Lett.* **104**, 235002 (2010).
- [32] J. D. Williams, *Phys. Rev. E* **89**, 023105 (2014).
- [33] M. Schwabe, M. Rubin-Zuzic, S. Zhdanov, H. M. Thomas, and G. E. Morfill, *Phys. Rev. Lett.* **99**, 095002 (2007).
- [34] S. Zhdanov, M. Schwabe C. Räth, H. M. Thomas, and G. E. Morfill, *Europhys. Lett.* **110**, 35001 (2015).
- [35] P. K. Shukla and B. Eliasson, *Rev. Mod. Phys.* **81**, 25 (2009).
- [36] P. Bandyopadhyay, G. Prasad, A. Sen, and P. K. Kaw, *Phys. Rev. Lett.* **101**, 065006 (2008).
- [37] Y. Nakamura, H. Bailung, and P. K. Shukla, *Phys. Rev. Lett.* **83**, 1602 (1999).
- [38] Y. Y. Tsai, J. Y. Tsai, and L. I, *Nat. Phys.* **12**, 573 (2016).
- [39] P.-C. Lin and L. I, *Phys. Rev. Lett.* **120**, 135004 (2018).
- [40] S. Knist, F. Greiner, F. Biss, and A. Piel, *Contrib. Plasma Phys.* **51**, 769 (2011).
- [41] J. Davidsen, M. Zhan, and R. Kapral, *Phys. Rev. Lett.* **101**, 208302 (2008).
- [42] J. Hardoüin, R. Hughes, A. Doostmohammadi, J. Laurent, T. Lopez-Leon, J. M. Yeomans, J. Ignés-Mullol, and F. Sagués, *Commun. Phys.* **2**, 121 (2019).